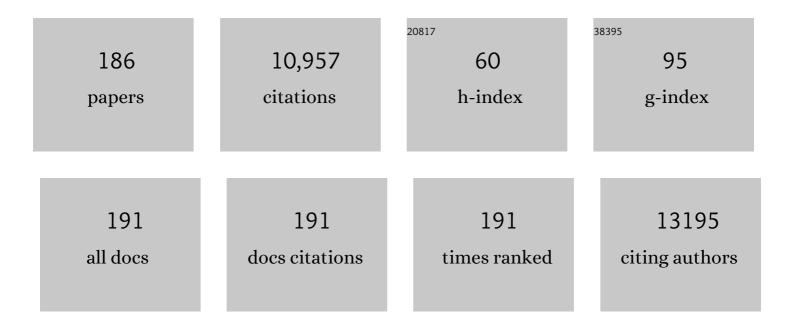
Shengbo Zhang

List of Publications by Year in descending order

Source: https://exaly.com/author-pdf/9309182/publications.pdf Version: 2024-02-01



#	Article	IF	CITATIONS
1	Cobalt Covalent Doping in MoS ₂ to Induce Bifunctionality of Overall Water Splitting. Advanced Materials, 2018, 30, e1801450.	21.0	402
2	Potassiumâ€Ionâ€Assisted Regeneration of Active Cyano Groups in Carbon Nitride Nanoribbons: Visibleâ€Lightâ€Driven Photocatalytic Nitrogen Reduction. Angewandte Chemie - International Edition, 2019, 58, 16644-16650.	13.8	356
3	Enhanced visible-light-driven photocatalytic inactivation of Escherichia coli using g-C3N4/TiO2 hybrid photocatalyst synthesized using a hydrothermal-calcination approach. Water Research, 2015, 86, 17-24.	11.3	323
4	Co/Co9S8@S,N-doped porous graphene sheets derived from S, N dual organic ligands assembled Co-MOFs as superior electrocatalysts for full water splitting in alkaline media. Nano Energy, 2016, 30, 93-102.	16.0	260
5	3D graphene/l̂´-MnO ₂ aerogels for highly efficient and reversible removal of heavy metal ions. Journal of Materials Chemistry A, 2016, 4, 1970-1979.	10.3	257
6	Bifunctional NH ₂ -MIL-88(Fe) metal–organic framework nanooctahedra for highly sensitive detection and efficient removal of arsenate in aqueous media. Journal of Materials Chemistry A, 2017, 5, 23794-23804.	10.3	230
7	Co/CoO nanoparticles immobilized on Co–N-doped carbon as trifunctional electrocatalysts for oxygen reduction, oxygen evolution and hydrogen evolution reactions. Chemical Communications, 2016, 52, 5946-5949.	4.1	221
8	Metal-organic framework derived nitrogen-doped porous carbon@graphene sandwich-like structured composites as bifunctional electrocatalysts for oxygen reduction and evolution reactions. Carbon, 2016, 106, 74-83.	10.3	206
9	A self-sponsored doping approach for controllable synthesis of S and N co-doped trimodal-porous structured graphitic carbon electrocatalysts. Energy and Environmental Science, 2014, 7, 3720-3726.	30.8	198
10	One-step synthesis of cobalt-doped MoS ₂ nanosheets as bifunctional electrocatalysts for overall water splitting under both acidic and alkaline conditions. Chemical Communications, 2018, 54, 3859-3862.	4.1	196
11	Biomass-derived N-doped porous carbon as electrode materials for Zn-air battery powered capacitive deionization. Chemical Engineering Journal, 2018, 334, 1270-1280.	12.7	182
12	Efficient Synthesis of Furfuryl Alcohol from H ₂ -Hydrogenation/Transfer Hydrogenation of Furfural Using Sulfonate Group Modified Cu Catalyst. ACS Sustainable Chemistry and Engineering, 2017, 5, 2172-2180.	6.7	177
13	Dramatically Enhanced Ambient Ammonia Electrosynthesis Performance by Inâ€Operando Created Li–S Interactions on MoS ₂ Electrocatalyst. Advanced Energy Materials, 2019, 9, 1803935.	19.5	176
14	Electrocatalytically Active Feâ€(Oâ€C ₂) ₄ Singleâ€Atom Sites for Efficient Reduction of Nitrogen to Ammonia. Angewandte Chemie - International Edition, 2020, 59, 13423-13429.	13.8	161
15	Size Modulation of Zirconium-Based Metal Organic Frameworks for Highly Efficient Phosphate Remediation. ACS Applied Materials & Interfaces, 2017, 9, 32151-32160.	8.0	146
16	β-FeOOH Nanorods/Carbon Foam-Based Hierarchically Porous Monolith for Highly Effective Arsenic Removal. ACS Applied Materials & Interfaces, 2017, 9, 13480-13490.	8.0	143
17	Ambient Electrosynthesis of Ammonia on a Biomass-Derived Nitrogen-Doped Porous Carbon Electrocatalyst: Contribution of Pyridinic Nitrogen. ACS Energy Letters, 2019, 4, 377-383.	17.4	142
18	NiFe-Layered Double Hydroxide Nanosheet Arrays Supported on Carbon Cloth for Highly Sensitive Detection of Nitrite, ACS Applied Materials & amp: Interfaces, 2018, 10, 6541-6551	8.0	140

#	Article	IF	CITATIONS
19	Nitrogenâ€Doped Carbon Nanotube Confined Co–N <i>_x</i> Sites for Selective Hydrogenation of Biomassâ€Derived Compounds. Advanced Materials, 2019, 31, e1808341.	21.0	138
20	Cu doping in CeO ₂ to form multiple oxygen vacancies for dramatically enhanced ambient N ₂ reduction performance. Chemical Communications, 2019, 55, 2952-2955.	4.1	138
21	Hydrothermal Transformation of Dried Grass into Graphitic Carbonâ€Based High Performance Electrocatalyst for Oxygen Reduction Reaction. Small, 2014, 10, 3371-3378.	10.0	135
22	Facile fabrication of composition-tunable Fe/Mg bimetal-organic frameworks for exceptional arsenate removal. Chemical Engineering Journal, 2019, 357, 579-588.	12.7	124
23	Fe/Fe2O3 nanoparticles anchored on Fe-N-doped carbon nanosheets as bifunctional oxygen electrocatalysts for rechargeable zinc-air batteries. Nano Research, 2016, 9, 2123-2137.	10.4	116
24	Simultaneously high-rate furfural hydrogenation and oxidation upgrading on nanostructured transition metal phosphides through electrocatalytic conversion at ambient conditions. Applied Catalysis B: Environmental, 2019, 244, 899-908.	20.2	115
25	Surface hydrogen bonding can enhance photocatalytic H2 evolution efficiency. Journal of Materials Chemistry A, 2013, 1, 14089.	10.3	113
26	Atomic Tuning of Single-Atom Fe–N–C Catalysts with Phosphorus for Robust Electrochemical CO ₂ Reduction. Nano Letters, 2022, 22, 1557-1565.	9.1	111
27	Anatase TiO ₂ Crystal Facet Growth: Mechanistic Role of Hydrofluoric Acid and Photoelectrocatalytic Activity. ACS Applied Materials & Interfaces, 2011, 3, 2472-2478.	8.0	108
28	S,N-Containing Co-MOF derived Co ₉ S ₈ @S,N-doped carbon materials as efficient oxygen electrocatalysts and supercapacitor electrode materials. Inorganic Chemistry Frontiers, 2017, 4, 491-498.	6.0	108
29	Hierarchical iron containing γ-MnO 2 hollow microspheres: A facile one-step synthesis and effective removal of As(III) via oxidation and adsorption. Chemical Engineering Journal, 2016, 301, 139-148.	12.7	106
30	A Facile Vapor-Phase Hydrothermal Method for Direct Growth of Titanate Nanotubes on a Titanium Substrate via a Distinctive Nanosheet Roll-Up Mechanism. Journal of the American Chemical Society, 2011, 133, 19032-19035.	13.7	99
31	One-step solid phase synthesis of a highly efficient and robust cobalt pentlandite electrocatalyst for the oxygen evolution reaction. Journal of Materials Chemistry A, 2016, 4, 18314-18321.	10.3	97
32	Shrimp-shell derived carbon nanodots as carbon and nitrogen sources to fabricate three-dimensional N-doped porous carbon electrocatalysts for the oxygen reduction reaction. Physical Chemistry Chemical Physics, 2016, 18, 4095-4101.	2.8	97
33	Macroscale cobalt-MOFs derived metallic Co nanoparticles embedded in N-doped porous carbon layers as efficient oxygen electrocatalysts. Applied Surface Science, 2017, 392, 402-409.	6.1	92
34	Fe o Alloyed Nanoparticles Catalyzing Efficient Hydrogenation of Cinnamaldehyde to Cinnamyl Alcohol in Water. Angewandte Chemie - International Edition, 2020, 59, 23521-23526.	13.8	91
35	Strongly Coupled CoCr ₂ O ₄ /Carbon Nanosheets as High Performance Electrocatalysts for Oxygen Evolution Reaction. Small, 2016, 12, 2866-2871.	10.0	90
36	Carbon-embedded Ni nanocatalysts derived from MOFs by a sacrificial template method for efficient hydrogenation of furfural to tetrahydrofurfuryl alcohol. Dalton Transactions, 2017, 46, 6358-6365.	3.3	88

#	Article	IF	CITATIONS
37	Formation of BNC Coordination to Stabilize the Exposed Active Nitrogen Atoms in gâ€C ₃ N ₄ for Dramatically Enhanced Photocatalytic Ammonia Synthesis Performance. Small, 2020, 16, e1906880.	10.0	88
38	Directly Hydrothermal Growth of Single Crystal Nb ₃ O ₇ (OH) Nanorod Film for High Performance Dye‧ensitized Solar Cells. Advanced Materials, 2012, 24, 1598-1603.	21.0	86
39	In situ growth of α-Fe ₂ O ₃ nanorod arrays on 3D carbon foam as an efficient binder-free electrode for highly sensitive and specific determination of nitrite. Journal of Materials Chemistry A, 2017, 5, 4726-4736.	10.3	86
40	Hierarchical MgFe-layered double hydroxide microsphere/graphene composite for simultaneous electrochemical determination of trace Pb(II) and Cd(II). Chemical Engineering Journal, 2018, 347, 953-962.	12.7	86
41	Vertically aligned nanorod-like rutileTiO2 single crystal nanowire bundles with superior electron transport and photoelectrocatalytic properties. Journal of Materials Chemistry, 2012, 22, 2465-2472.	6.7	84
42	One-step synthesis of nitrogen-doped microporous carbon materials as metal-free electrocatalysts for oxygen reduction reaction. Journal of Materials Chemistry A, 2014, 2, 11666-11671.	10.3	84
43	Single crystal α-Fe2O3 with exposed {104} facets for high performance gas sensor applications. RSC Advances, 2012, 2, 6178.	3.6	82
44	Directly hydrothermal growth of ultrathin MoS2 nanostructured films as high performance counter electrodes for dye-sensitised solar cells. RSC Advances, 2014, 4, 21277.	3.6	82
45	Highly Ordered Single Crystalline Nanowire Array Assembled Three-Dimensional Nb ₃ O ₇ (OH) and Nb ₂ O ₅ Superstructures for Energy Storage and Conversion Applications. ACS Nano, 2016, 10, 507-514.	14.6	81
46	Highly selective liquid-phase hydrogenation of furfural over N-doped carbon supported metallic nickel catalyst under mild conditions. Molecular Catalysis, 2017, 429, 51-59.	2.0	81
47	Nitrogen-free commercial carbon cloth with rich defects for electrocatalytic ammonia synthesis under ambient conditions. Chemical Communications, 2018, 54, 11188-11191.	4.1	79
48	Ethanol introduced synthesis of ultrastable 1T-MoS2 for removal of Cr(VI). Journal of Hazardous Materials, 2020, 394, 122525.	12.4	79
49	Two-dimensional CoNi nanoparticles@S,N-doped carbon composites derived from S,N-containing Co/Ni MOFs for high performance supercapacitors. Journal of Materials Chemistry A, 2017, 5, 9873-9881.	10.3	75
50	Determination of Iodide via Direct Fluorescence Quenching at Nitrogen-Doped Carbon Quantum Dot Fluorophores. Environmental Science and Technology Letters, 2014, 1, 87-91.	8.7	74
51	Density Functional Studies of Stoichiometric Surfaces of Orthorhombic Hybrid Perovskite CH ₃ NH ₃ Pbl ₃ . Journal of Physical Chemistry C, 2015, 119, 1136-1145.	3.1	73
52	High-Efficiency Co/Co _{<i>x</i>} S _{<i>y</i>} @S,N-Codoped Porous Carbon Electrocatalysts Fabricated from Controllably Grown Sulfur- and Nitrogen-Including Cobalt-Based MOFs for Rechargeable Zinc–Air Batteries. ACS Applied Materials & Interfaces, 2017, 9, 34269-34278.	8.0	71
53	Hierarchical Porous Carbon Materials Derived from Kelp for Superior Capacitive Applications. ACS Sustainable Chemistry and Engineering, 2019, 7, 8735-8743.	6.7	71
54	Facile Fabrication of Anatase TiO ₂ Microspheres on Solid Substrates and Surface Crystal Facet Transformation from {001} to {101}. Chemistry - A European Journal, 2011, 17, 5949-5957.	3.3	70

#	Article	IF	CITATIONS
55	Co ₉ S ₈ @N,P-doped porous carbon electrocatalyst using biomass-derived carbon nanodots as a precursor for overall water splitting in alkaline media. RSC Advances, 2017, 7, 19181-19188.	3.6	69
56	Ambient Electrosynthesis of Ammonia on a Core–Shell‧tructured Au@CeO ₂ Catalyst: Contribution of Oxygen Vacancies in CeO ₂ . Chemistry - A European Journal, 2019, 25, 5904-5911.	3.3	69
57	Spontaneous Redox Approach to the Self-Assembly Synthesis of Au/CeO ₂ Plasmonic Photocatalysts with Rich Oxygen Vacancies for Selective Photocatalytic Conversion of Alcohols. ACS Applied Materials & Interfaces, 2018, 10, 31394-31403.	8.0	67
58	A fluorescent chitosan hydrogel detection platform for the sensitive and selective determination of trace mercury(<scp>ii</scp>) in water. Journal of Materials Chemistry A, 2015, 3, 19455-19460.	10.3	66
59	3D Fe ₃ O ₄ @Au@Ag nanoflowers assembled magnetoplasmonic chains for in situ SERS monitoring of plasmon-assisted catalytic reactions. Journal of Materials Chemistry A, 2016, 4, 8866-8874.	10.3	63
60	Europium-based infinite coordination polymer nanospheres as an effective fluorescence probe for phosphate sensing. RSC Advances, 2017, 7, 8661-8669.	3.6	62
61	Vapour-phase hydrothermal synthesis of Ni2P nanocrystallines on carbon fiber cloth for high-efficiency H2 production and simultaneous urea decomposition. Electrochimica Acta, 2017, 254, 44-49.	5.2	62
62	Highly Dispersed Copper Nanoparticles Supported on Activated Carbon as an Efficient Catalyst for Selective Reduction of Vanillin. Small, 2018, 14, e1801953.	10.0	62
63	Fabrication of hierarchical iron-containing MnO ₂ hollow microspheres assembled by thickness-tunable nanosheets for efficient phosphate removal. Journal of Materials Chemistry A, 2016, 4, 14814-14826.	10.3	60
64	Selective Determination of Cr(VI) by Glutaraldehyde Cross-Linked Chitosan Polymer Fluorophores. ACS Sensors, 2018, 3, 792-798.	7.8	60
65	A hierarchical hybrid monolith: MoS ₄ ^{2â^'} -intercalated NiFe layered double hydroxide nanosheet arrays assembled on carbon foam for highly efficient heavy metal removal. Journal of Materials Chemistry A, 2019, 7, 12869-12881.	10.3	58
66	Visible light active pure rutile TiO2 photoanodes with 100% exposed pyramid-shaped (111) surfaces. Nano Research, 2012, 5, 762-769.	10.4	57
67	Vaporâ€Phase Hydrothermal Transformation of HTiOF ₃ Intermediates into {001} Faceted Anatase Singleâ€Crystalline Nanosheets. Small, 2012, 8, 3664-3673.	10.0	56
68	Vapor-phase hydrothermal growth of single crystalline NiS2 nanostructure film on carbon fiber cloth for electrocatalytic oxidation of alcohols to ketones and simultaneous H2 evolution. Nano Research, 2018, 11, 1004-1017.	10.4	56
69	Liberating Nâ€CNTs Confined Highly Dispersed CoN <i>_x</i> Sites for Selective Hydrogenation of Quinolines. Advanced Materials, 2019, 31, e1906051.	21.0	56
70	Ultrafine nickel–cobalt alloy nanoparticles incorporated into three-dimensional porous graphitic carbon as an electrode material for supercapacitors. Journal of Materials Chemistry A, 2016, 4, 17080-17086.	10.3	53
71	Manipulating solar absorption and electron transport properties of rutile TiO2 photocatalysts via highly n-type F-doping. Journal of Materials Chemistry A, 2014, 2, 3513.	10.3	52
72	Rutile TiO2 microspheres with exposed nano-acicular single crystals for dye-sensitized solar cells. Nano Research, 2011, 4, 938-947.	10.4	50

#	Article	IF	CITATIONS
73	Enhanced fluoride removal by hierarchically porous carbon foam monolith with high loading of UiO-66. Journal of Colloid and Interface Science, 2019, 542, 269-280.	9.4	50
74	Lignosulfonate functionalized g-C ₃ N ₄ /carbonized wood sponge for highly efficient heavy metal ion scavenging. Journal of Materials Chemistry A, 2020, 8, 12687-12698.	10.3	48
75	An in situ vapour phase hydrothermal surface doping approach for fabrication of high performance Co ₃ O ₄ electrocatalysts with an exceptionally high S-doped active surface. Chemical Communications, 2015, 51, 5695-5697.	4.1	47
76	The surface sulfur doping induced enhanced performance of cobalt catalysts in oxygen evolution reactions. Chemical Communications, 2016, 52, 9450-9453.	4.1	47
77	Highly dispersed Co and Ni nanoparticles encapsulated in N-doped carbon nanotubes as efficient catalysts for the reduction of unsaturated oxygen compounds in aqueous phase. Catalysis Science and Technology, 2018, 8, 5506-5514.	4.1	47
78	Vapor-phase hydrothermal transformation of a nanosheet array structure Ni(OH) ₂ into ultrathin Ni ₃ S ₂ nanosheets on nickel foam for high-efficiency overall water splitting. Journal of Materials Chemistry A, 2018, 6, 19201-19209.	10.3	47
79	In Situ Synthesis of Highly Dispersed Cu–Co Bimetallic Nanoparticles for Tandem Hydrogenation/Rearrangement of Bioderived Furfural in Aqueous-Phase. ACS Sustainable Chemistry and Engineering, 2018, 6, 14919-14925.	6.7	46
80	Fabrication of hierarchically porous NH2-MIL-53/wood-carbon hybrid membrane for highly effective and selective sequestration of Pb2+. Chemical Engineering Journal, 2020, 387, 124141.	12.7	44
81	Selective electrocatalytic hydrogenation of nitrobenzene over copper-platinum alloying catalysts: Experimental and theoretical studies. Applied Catalysis B: Environmental, 2021, 298, 120545.	20.2	44
82	An efficient and reusable bimetallic Ni3Fe NPs@C catalyst for selective hydrogenation of biomass-derived levulinic acid to γ-valerolactone. Chinese Journal of Catalysis, 2018, 39, 1599-1607.	14.0	43
83	Theoretical study of single transition metal atom modified MoP as a nitrogen reduction electrocatalyst. Physical Chemistry Chemical Physics, 2019, 21, 5950-5955.	2.8	43
84	Selective Pseudocapacitive Deionization of Calcium Ions in Copper Hexacyanoferrate. ACS Applied Materials & Interfaces, 2020, 12, 41437-41445.	8.0	43
85	Encapsulated Ni-Co alloy nanoparticles as efficient catalyst for hydrodeoxygenation of biomass derivatives in water. Chinese Journal of Catalysis, 2021, 42, 2027-2037.	14.0	43
86	MoS ₂ Nanodots Anchored on Reduced Graphene Oxide for Efficient N ₂ Fixation to NH ₃ . ACS Sustainable Chemistry and Engineering, 2020, 8, 2320-2326.	6.7	42
87	Efficient electrochemical N ₂ fixation by doped-oxygen-induced phosphorus vacancy defects on copper phosphide nanosheets. Journal of Materials Chemistry A, 2020, 8, 5936-5942.	10.3	40
88	Rutile TiO2 films with 100% exposed pyramid-shaped (111) surface: photoelectron transport properties under UV and visible light irradiation. Journal of Materials Chemistry A, 2013, 1, 2646.	10.3	39
89	Experimental and theoretical understanding on electrochemical activation and inactivation processes of Nb ₃ O ₇ (OH) for ambient electrosynthesis of NH ₃ . Journal of Materials Chemistry A, 2019, 7, 16969-16978.	10.3	39
90	Anatase TiO2 mesocrystals with exposed (001) surface for enhanced photocatalytic decomposition capability toward gaseous styrene. Catalysis Today, 2014, 224, 216-224.	4.4	38

#	Article	IF	CITATIONS
91	Ambient Electrosynthesis of Ammonia Using Core–Shell Structured Au@C Catalyst Fabricated by One-Step Laser Ablation Technique. ACS Applied Materials & Interfaces, 2019, 11, 44186-44195.	8.0	38
92	Plasma-etching enhanced titanium oxynitride active phase with high oxygen content for ambient electrosynthesis of ammonia. Electrochemistry Communications, 2019, 100, 90-95.	4.7	38
93	Hierarchically porous poly(amidoxime)/bacterial cellulose composite aerogel for highly efficient scavenging of heavy metals. Journal of Colloid and Interface Science, 2021, 600, 752-763.	9.4	38
94	Self-assembled Pd/CeO2 catalysts by a facile redox approach for high-efficiency hydrogenation of levulinic acid into gamma-valerolactone. Catalysis Communications, 2017, 93, 10-14.	3.3	37
95	Efficient electrocatalytic nitrogen reduction to ammonia with aqueous silver nanodots. Communications Chemistry, 2021, 4, .	4.5	36
96	Improved UV resistance in wood through the hydrothermal growth of highly ordered ZnO nanorod arrays. Journal of Materials Science, 2012, 47, 4457-4462.	3.7	35
97	In Situ Growth of Ultrathin Ni(OH) ₂ Nanosheets as Catalyst for Electrocatalytic Oxidation Reactions. ChemSusChem, 2021, 14, 2935-2942.	6.8	35
98	Electrodeposition of hierarchically amorphous FeOOH nanosheets on carbonized bamboo as an efficient filter membrane for As(III) removal. Chemical Engineering Journal, 2020, 392, 123773.	12.7	34
99	A three-dimensional porous Co@C/carbon foam hybrid monolith for exceptional oil–water separation. Nanoscale, 2019, 11, 12161-12168.	5.6	33
100	Highly selective capacitive deionization of copper ions in FeS2@N, S co-doped carbon electrode from wastewater. Separation and Purification Technology, 2021, 262, 118336.	7.9	33
101	Highly efficient electrocatalytic oxidation of urea on a Mn-incorporated Ni(OH) ₂ /carbon fiber cloth for energy-saving rechargeable Zn–air batteries. Chemical Communications, 2017, 53, 10711-10714.	4.1	32
102	Engineering the band gap of bare titanium dioxide materials for visible-light activity: a theoretical prediction. RSC Advances, 2013, 3, 8777.	3.6	31
103	Transformation of carbon-encapsulated metallic Co into ultrafine Co/CoO nanoparticles exposed on N-doped graphitic carbon for high-performance rechargeable zinc-air battery. Applied Surface Science, 2018, 448, 369-379.	6.1	31
104	Electrochemical reduction of nitrate to ammonia in a fluidized electrocatalysis system with oxygen vacancy-rich CuO _{<i>x</i>) sub> nanoparticles. Inorganic Chemistry Frontiers, 2021, 8, 5209-5213.}	6.0	31
105	A highly crystalline Nb3O7F nanostructured photoelectrode: fabrication and photosensitisation. Journal of Materials Chemistry A, 2013, 1, 6563.	10.3	29
106	Cobalt single atom catalysts for the efficient electrosynthesis of hydrogen peroxide. Inorganic Chemistry Frontiers, 2021, 8, 2829-2834.	6.0	29
107	Shrimp-shell derived carbon nanodots as precursors to fabricate Fe,N-doped porous graphitic carbon electrocatalysts for efficient oxygen reduction in zinc–air batteries. Inorganic Chemistry Frontiers, 2016, 3, 910-918.	6.0	27
108	Hollow mesoporous SiO ₂ sphere nanoarchitectures with encapsulated silver nanoparticles for catalytic reduction of 4-nitrophenol. Inorganic Chemistry Frontiers, 2016, 3, 663-670.	6.0	27

#	Article	IF	CITATIONS
109	Carbon-encapsulated heazlewoodite nanoparticles as highly efficient and durable electrocatalysts for oxygen evolution reactions. Nano Research, 2017, 10, 3522-3533.	10.4	27
110	Electrocatalytic oxidation of benzyl alcohol for simultaneously promoting H ₂ evolution by a Co _{0.83} Ni _{0.17} /activated carbon electrocatalyst. New Journal of Chemistry, 2018, 42, 6381-6388.	2.8	27
111	Porous carbon nanosheets functionalized with Fe ₃ O ₄ nanoparticles for capacitive removal of heavy metal ions from water. Environmental Science: Water Research and Technology, 2020, 6, 331-340.	2.4	27
112	Hierarchical Porous Iron Metal–Organic Gel/Bacterial Cellulose Aerogel: Ultrafast, Scalable, Room-Temperature Aqueous Synthesis, and Efficient Arsenate Removal. ACS Applied Materials & Interfaces, 2021, 13, 47684-47695.	8.0	27
113	Nature of visible-light responsive fluorinated titanium dioxides. Journal of Materials Chemistry A, 2013, 1, 12948.	10.3	26
114	Potassiumâ€lonâ€Assisted Regeneration of Active Cyano Groups in Carbon Nitride Nanoribbons: Visibleâ€Lightâ€Driven Photocatalytic Nitrogen Reduction. Angewandte Chemie, 2019, 131, 16797-16803.	2.0	26
115	{001} facets dominated anatase TiO2: Morphology, formation/etching mechanisms and performance. Science China Chemistry, 2013, 56, 402-417.	8.2	24
116	Vapor-phase hydrothermal synthesis of rutile TiO2 nanostructured film with exposed pyramid-shaped (1 1 1) surface and superiorly photoelectrocatalytic performance. Journal of Colloid and Interface Science, 2014, 429, 53-61.	9.4	24
117	Zirconium metal organic frameworks-based DGT technique for in situ measurement of dissolved reactive phosphorus in waters. Water Research, 2018, 147, 223-232.	11.3	24
118	An oxygen-coordinated molybdenum single atom catalyst for efficient electrosynthesis of ammonia. Chemical Communications, 2021, 57, 5410-5413.	4.1	24
119	A pyrolysis–phosphorization approach to fabricate carbon nanotubes with embedded CoP nanoparticles for ambient electrosynthesis of ammonia. Chemical Communications, 2019, 55, 12376-12379.	4.1	23
120	Electrocatalytically Active Feâ€(O ₂) ₄ Singleâ€Atom Sites for Efficient Reduction of Nitrogen to Ammonia. Angewandte Chemie, 2020, 132, 13525-13531.	2.0	23
121	Adsorption and oxidation of oxalic acid on anatase TiO2 (001) surface: A density functional theory study. Journal of Colloid and Interface Science, 2015, 454, 180-186.	9.4	22
122	Sulfonate group modified Ni catalyst for highly efficient liquid-phase selective hydrogenation of bio-derived furfural. Chinese Chemical Letters, 2018, 29, 1617-1620.	9.0	22
123	Hollow carbon sphere encapsulated nickel nanoreactor for aqueous-phase hydrogenation-rearrangement tandem reaction with enhanced catalytic performance. Applied Catalysis B: Environmental, 2022, 306, 121140.	20.2	22
124	Switching the photocatalytic activity of g-C3N4 by homogenous surface chemical modification with nitrogen residues and vacancies. RSC Advances, 2015, 5, 21430-21433.	3.6	21
125	Converting eggplant biomass into multifunctional porous carbon electrodes for self-powered capacitive deionization. Environmental Science: Water Research and Technology, 2019, 5, 1054-1063.	2.4	21
126	Enhancement of the visible-light photocatalytic activity of CeO ₂ by chemisorbed oxygen in the selective oxidation of benzyl alcohol. New Journal of Chemistry, 2019, 43, 7355-7362.	2.8	21

#	Article	IF	CITATIONS
127	Pseudocapacitive desalination via valence engineering with spindle-like manganese oxide/carbon composites. Nano Research, 2021, 14, 4878-4884.	10.4	21
128	A New Vaporâ€Phase Hydrothermal Method to Concurrently Grow ZnO Nanotube and Nanorod Array Films on Different Sides of a Zinc Foil Substrate. Chemistry - A European Journal, 2012, 18, 5165-5169.	3.3	20
129	Adenovirus inactivation by in situ photocatalytically and photoelectrocatalytically generated halogen viricides. Chemical Engineering Journal, 2014, 253, 538-543.	12.7	20
130	Intrinsic Pseudocapacitive Affinity in Manganese Spinel Ferrite Nanospheres for High-Performance Selective Capacitive Removal of Ca ²⁺ and Mg ²⁺ . ACS Applied Materials & Interfaces, 2021, 13, 38886-38896.	8.0	20
131	Growth and in situ transformation of TiO2 and HTiOF3 crystals on chitosan-polyvinyl alcohol co-polymer substrates under vapor phase hydrothermal conditions. Nano Research, 2016, 9, 745-754.	10.4	19
132	A sulfonate group functionalized active carbon-based Cu catalyst for electrochemical ammonia synthesis under ambient conditions. Inorganic Chemistry Frontiers, 2019, 6, 2832-2836.	6.0	19
133	Laser Irradiation in Liquid to Release Cobalt Single-Atom Sites for Efficient Electrocatalytic N2 Reduction. ACS Applied Energy Materials, 2020, 3, 6079-6086.	5.1	19
134	Robust enhanced hydrogen production at acidic conditions over molybdenum oxides-stabilized ultrafine palladium electrocatalysts. Nano Research, 2021, 14, 268-274.	10.4	19
135	Geometric structure of rutile titanium dioxide (111) surfaces. Physical Review B, 2014, 90, .	3.2	18
136	Highly sensitive detection of nitrite by using gold nanoparticle-decorated α-Fe ₂ O ₃ nanorod arrays as self-supporting photo-electrodes. Inorganic Chemistry Frontiers, 2019, 6, 1432-1441.	6.0	18
137	Converting Co2+-impregnated g-C3N4 into N-doped CNTs-confined Co nanoparticles for efficient hydrogenation rearrangement reactions of furanic aldehydes. Nano Research, 2021, 14, 2846-2852.	10.4	18
138	Photoelectrochemical determination of intrinsic kinetics of photoelectrocatalysis processes at {001} faceted anatase TiO ₂ photoanodes. RSC Advances, 2015, 5, 12860-12865.	3.6	17
139	One-pot redox synthesis of Pt/Fe ₃ O ₄ catalyst for efficiently chemoselective hydrogenation of cinnamaldehyde. RSC Advances, 2017, 7, 21107-21113.	3.6	17
140	Efficiently electrocatalytic oxidation of benzyl alcohol for energy- saved zinc-air battery using a multifunctional nickel–cobalt alloy electrocatalyst. Journal of Colloid and Interface Science, 2018, 532, 37-46.	9.4	17
141	Highly dispersed nickel anchored on a N-doped carbon molecular sieve derived from metal–organic frameworks for efficient hydrodeoxygenation in the aqueous phase. Chemical Communications, 2020, 56, 6696-6699.	4.1	17
142	Tunable synthesis of imines and secondary-amines from tandem hydrogenation-coupling of aromatic nitro and aldehyde over NiCo5 bi-metallic catalyst. Applied Catalysis B: Environmental, 2021, 280, 119448.	20.2	17
143	Synchronous removal of tetracycline and water hardness ions by capacitive deionization. Journal of Cleaner Production, 2021, 316, 128251.	9.3	17
144	Electrochemical deposition of Pt on carbon fiber cloth utilizing Pt mesh counter electrode during hydrogen evolution reaction for electrocatalytic hydrogenation reduction of p-nitrophenol. New Journal of Chemistry, 2017, 41, 7012-7019.	2.8	16

#	Article	IF	CITATIONS
145	Selective Growth of Highâ€Density Anatase {101} Twin Boundaries on Highâ€Energy {001} Facets. Small Structures, 2020, 1, 2000025.	12.0	16
146	High-performance pseudocapacitive removal of cadmium via synergistic valence conversion in perovskite-type FeMnO3. Journal of Hazardous Materials, 2022, 439, 129575.	12.4	16
147	Photoelectrochemical manifestation of intrinsic photoelectron transport properties of vertically aligned {001} faceted single crystal TiO ₂ nanosheet films. RSC Advances, 2015, 5, 55438-55444.	3.6	15
148	A nanoparticulate liquid binding phase based DGT device for aquatic arsenic measurement. Talanta, 2016, 160, 225-232.	5.5	15
149	Metal (Co/Mo)–N bond anchor-doped N in porous carbon for electrochemical nitrogen reduction. Inorganic Chemistry Frontiers, 2021, 8, 1476-1481.	6.0	15
150	Sustainable 2,5-furandicarboxylic synthesis by a direct 5-hydroxymethylfurfural fuel cell based on a bifunctional PtNiS _x catalyst. Chemical Communications, 2020, 56, 13611-13614.	4.1	15
151	Ambient Electrochemical Nitrogen Fixation over a Bifunctional Mo–(O–C ₂) ₄ Site Catalyst. Journal of Physical Chemistry C, 2022, 126, 965-973.	3.1	15
152	Simultaneous Separation and Recovery of Gold and Copper from Electronic Waste Enabled by an Asymmetric Electrochemical System. ACS Applied Materials & Interfaces, 2022, 14, 9544-9556.	8.0	15
153	Enhanced Desalination Performance by a Novel Archimedes Spiral Flow Channel for Flow-Electrode Capacitive Deionization. ACS ES&T Engineering, 2022, 2, 1250-1259.	7.6	15
154	Efficient Synthesis of 2-Methylfuran from Bio-Derived Furfural over Supported Copper Catalyst: The Synergistic Effect of CuO _x and Cu. ChemistrySelect, 2017, 2, 9984-9991.	1.5	14
155	Bacterial cellulose hybrid membrane grafted with high ratio of adipic dihydrazide for highly efficient and selective recovery of gold from e-waste. Separation and Purification Technology, 2022, 292, 121021.	7.9	14
156	Integration of Fe2O3-based photoanode and atomically dispersed cobalt cathode for efficient photoelectrochemical NH3 synthesis. Chinese Chemical Letters, 2021, 32, 805-810.	9.0	13
157	Enhanced photocatalytic activity of a hollow TiO ₂ –Au–TiO ₂ sandwich structured nanocomposite. RSC Advances, 2016, 6, 18958-18964.	3.6	12
158	Synergistic catalysis of cluster and atomic copper induced by copper-silica interface in transfer-hydrogenation. Nano Research, 2021, 14, 4601-4609.	10.4	12
159	Instant inactivation and rapid decomposition of Escherichia coli using a high efficiency TiO2 nanotube array photoelectrode. RSC Advances, 2013, 3, 20824.	3.6	11
160	Precisely controlled heterogeneous nucleation sites for TiO ₂ crystal growth. CrystEngComm, 2014, 16, 7502.	2.6	11
161	Threeâ€Dimensional Nâ€doped Porous Carbon Derived from Monosodium Glutamate for Capacitive Deionization and the Oxygen Reduction Reaction. ChemElectroChem, 2018, 5, 3873-3880.	3.4	10
162	The electrochemical corrosion of an air thermally-treated carbon fiber cloth electrocatalyst with outstanding oxygen evolution activity under alkaline conditions. Chemical Communications, 2019, 55, 2344-2347.	4.1	10

#	Article	IF	CITATIONS
163	CoO _x @Co Nanoparticleâ€based Catalyst for Efficient Selective Transfer Hydrogenation of α,βâ€Unsaturated Aldehydes. ChemCatChem, 2020, 12, 1019-1024.	3.7	10
164	Rational Design of Cobaltâ€Platinum Alloy Decorated Cobalt Nanoparticles for Oneâ€Pot Synthesis of Imines from Nitroarenes and Aldehydes. ChemCatChem, 2020, 12, 5948-5958.	3.7	10
165	A fluidized electrocatalysis approach for ammonia synthesis using oxygen vacancy-rich Co ₃ O ₄ nanoparticles. Inorganic Chemistry Frontiers, 2021, 8, 4026-4034.	6.0	10
166	<i>In situ</i> transformation of Fe-doped Ni ₁₂ P ₅ into low-crystallized NiFe ₂ O ₄ with high-spin Fe ⁴⁺ for efficient electrocatalytic water oxidation. Journal of Materials Chemistry A, 2021, 9, 10289-10296.	10.3	10
167	Crystal plane effect of ceria on supported copper catalyst for liquid-phase hydrogenation of unsaturated aldehyde. Journal of Colloid and Interface Science, 2021, 596, 34-43.	9.4	10
168	The catalytic behaviour in aqueous-phase hydrogenation over a renewable Ni catalyst derived from a perovskite-type oxide. Dalton Transactions, 2018, 47, 17276-17284.	3.3	9
169	A universal route to fabricate bacterial cellulose-based composite membranes for simultaneous removal of multiple pollutants. Chemical Communications, 2021, 57, 8592-8595.	4.1	9
170	Facile synthesis of N, P co-doped carbon encapsulated Ni catalyst for green production of cyclopentanone from biomass derivative furfural. Fuel, 2022, 319, 123815.	6.4	9
171	Iron covalent doping in WB ₂ to boost its hydrogen evolution activity. Inorganic Chemistry Frontiers, 2022, 9, 524-530.	6.0	8
172	Ambient ammonia production via electrocatalytic nitrate reduction catalyzed by flower-like CuCo2O4 electrocatalyst. Inorganic Chemistry Frontiers, 0, , .	6.0	8
173	Pt-Modified MoO ₃ catalyst for the electrochemically selective Cî€O hydrogenation of cinnamaldehyde. Chemical Communications, 2022, 58, 6721-6724.	4.1	8
174	Oxoacetohydrazideâ€functionalized cellulose with enhanced adsorption performance. Journal of Applied Polymer Science, 2016, 133, .	2.6	7
175	Highly ordered Nb2O5 nanochannel film with rich oxygen vacancies for electrocatalytic N2 reduction: Inactivation and regeneration of electrode. Chinese Chemical Letters, 2021, 32, 2833-2836.	9.0	6
176	Copper-assisted growth of high-purity carbon nanofiber networks with controllably tunable wettabilities. Journal of Materials Chemistry A, 2021, 9, 22039-22047.	10.3	6
177	<i>In situ</i> growth of MOFs on Ni(OH) ₂ for efficient electrocatalytic oxidation of 5-hydroxymethylfurfural. Chemical Communications, 2021, 57, 11358-11361.	4.1	6
178	Bacterial cellulose-regulated synthesis of metallic Ni catalysts for high-efficiency electrosynthesis of hydrogen peroxide. Science China Materials, 0, , 1.	6.3	6
179	Copper nanocrystals anchored on an O-rich carbonized corn gel for nitrogen electroreduction to ammonia. Inorganic Chemistry Frontiers, 2020, 7, 3555-3560.	6.0	5
180	hcp-phased Ni nanoparticles with generic catalytic hydrogenation activities toward different functional groups. Science China Materials, 2022, 65, 1252-1261.	6.3	5

#	Article	IF	CITATIONS
181	A freestanding, hierarchically porous poly(imine dioxime) membrane enabling selective gold recovery from eâ€waste with unprecedented capacity. EcoMat, 2022, 4, .	11.9	5
182	Carbothermal Methods: Highly Dispersed Copper Nanoparticles Supported on Activated Carbon as an Efficient Catalyst for Selective Reduction of Vanillin (Small 36/2018). Small, 2018, 14, 1870164.	10.0	4
183	Construction of Pd/BiOCl Catalyst for Highlyâ€selective Synthesis of Benzoin Ethyl Ether by Chlorine Promoted Coupling Reaction. ChemCatChem, 2019, 11, 2676-2682.	3.7	4
184	Gold-Modified Mo ₂ C Nanoparticles Supported on Nitrogen-Doped Carbon Nanotubes for Electrochemical Nitrogen Fixation. ACS Applied Nano Materials, 2022, 5, 7382-7391.	5.0	3
185	The morphology and optical properties of ZnO crystals fabricated by hydrothermal method under pulsed magnetic field. Physica Status Solidi C: Current Topics in Solid State Physics, 2013, 10, 1276-1279.	0.8	2
186	Fe o Alloyed Nanoparticles Catalyzing Efficient Hydrogenation of Cinnamaldehyde to Cinnamyl Alcohol in Water. Angewandte Chemie, 2020, 132, 23727-23732.	2.0	1